

Remarkable Thermal Contraction in Small Size Single-Walled Boron Nanotubes

Xianhu Zha^{1,2,3}, Shuang Li⁴, Ruiqin Zhang^{2,*} and Zijing Lin^{1,*}

¹ Department of Physics & Collaborative Innovation Center of Suzhou Nano Science and Technology, University of Science and Technology of China, Hefei 230026, China.

² Department of Physics and Materials Science, City University of Hong Kong, Kowloon Tong, Hong Kong.

³ USTC-CityU Joint Advanced Research Centre, Suzhou 215123, China.

⁴ Nano Structured Materials Center, Nanjing University of Science and Technology, Nanjing 210094, China.

Received 23 September 2013; Accepted (in revised version) 20 November 2013

Communicated by Michel A. Van Hove

Available online 10 April 2014

Abstract. Density functional theory combined with the Grüneisen approximation is used to calculate the thermal properties of single-walled boron nanotubes (BNTs). The specific heat and thermal expansion are investigated. The thermal expansion coefficient of the BNT is found to be significantly correlated with tube size and chirality. A remarkable thermal contraction is found at small tube diameters. These results indicate that BNTs would have potential applications in sensors, actuators, and memory materials.

AMS subject classifications: 80A17, 82-04

PACS: 65.40.Ba, 65.40.De, 65.80.-g

Key words: Density functional theory, Grüneisen approximation, single-walled boron nanotubes, remarkable thermal contraction.

1 Introduction

Since the discovery of the carbon nanotube (CNT) by Iijima in 1991 [1], the one-dimensional (1D) tube system has attracted considerable attention, due to its outstanding electronic and mechanical properties [2–4]. Although the CNT demonstrates excellent properties, it suffers from the key problem of controlling tube chirality during preparation [5]. This technical problem restricts many of its potential applications such as electrical conduction and field emission devices [6]. Other materials which are less dependent

*Corresponding author. *Email addresses:* aprqz@cityu.edu.hk (R. Zhang), zjlin@ustc.edu.cn (Z. Lin)

on chirality are therefore sought. Boron, as the neighboring element of carbon in the periodic table, has logically been of interest to scientists interested in this topic. It demonstrates many outstanding properties which are similar to carbon, such as low density and high melting point [7]. The 1D single-walled boron nanotube (BNT) was first fabricated by Ciuparu et al. as early as 2004 [8]. Later, Liu et al. synthesized multi-walled BNTs combined with boron nanowire [6]. There have also been plentiful theoretical studies of BNTs [9–17]. These predict that BNTs will have higher electrical conductivity and more storage capacity for hydrogen and lithium compared to CNTs [13,18,19]. In addition, the electrical properties of single-walled BNT are shown to have less chirality dependence. The single-walled BNT with a buckled triangular shape has been predicted to be metallic regardless of tube size and chirality [9–13]. The most stable single-walled BNTs [14–16] occur in the form of the hexagonal density $\eta=1/9$ (η = the number of hexagons/the number of triangles) with two- and three-center bonding, which structures have been found to be metallic at tube diameters larger than 17\AA [15]. The mechanical and electrical properties of this type of tube have been researched by Singh et al., who reported a stiffness of 210N/m [20]. Its electron transport has been researched by Lau et al., who showed that BNTs have lower resistance than single-walled CNTs of comparable length [21]. Because of their low chirality dependence, Liu et al. proposed that BNT would be superior to CNT in some aspects, for instance in field emission applications [6].

Due to these fascinating properties, BNTs are likely to have potential applications in the future development of nanoscale devices. Although their structural and electrical properties have been widely investigated [14–16,20,21], little work has been done on their thermal properties. In this paper, we therefore calculate the thermal properties of the single-walled BNTs, including the specific heat and thermal expansion, with the focus on the latter. We obtain a large negative thermal expansion for small tube diameter, which suggests an application for the BNT in counteracting the thermal expansion of normal materials in a BNT-based nanodevice. Moreover, our results indicate that BNTs would also be useful in sensors, actuators, and memory materials [22].

The rest of this paper is organized as follows. In Section 2 we present the theoretical and computational method. In Section 3 we discuss the thermal properties of BNTs and we summarize our work in Section 4.

2 Theoretical and computational method

In our study, the BNTs are calculated using density functional theory (DFT) [23] implemented in SIESTA code [24, 25] based on the Troullier-Martins pseudopotential. The generalized gradient approximation (GGA) [26] with Perdew-Burke-Ernzerhof (PBE) parameterization is used for the exchange and correlation functional. A basis set of double zeta polarizations (DZP) is employed, together with a plane-wave energy mesh cutoff of 240Ry and an energy shift of 0.02Ry . All systems are relaxed until the atomic forces are smaller than $0.001\text{eV}/\text{\AA}$. These parameters are crucial for structural optimization and

phonon dispersion computation. The BNTs are studied with periodic structures along the z -axis direction. A vacuum separation of 10\AA in the x - y plane is used to eliminate the interactions of neighboring tubes.

The quasi-harmonic approximation (QHA) method has been widely used in studying the thermal properties of nanomaterials [27]. Here, the QHA combined with the Grüneisen approach is chosen to study the thermal expansion coefficients (TECs) of BNTs. Since CNTs have already been comprehensively studied [28–32], the (5,5) CNT is used to confirm the accuracy of our approach. A supercell with five units along the z -axis of the (5,5) CNT and three units of each BNT is used to calculate phonon dispersion, since the atom number of each BNT unit cell is more than that of the (5,5) CNT. The atom number of each supercell is more than 100 [33], which is essential for calculating the phonon dispersion using the frozen phonon method in SIESTA. The phonon dispersion for each tube is calculated from $\Gamma(0,0,0)$ to $X(0,0,\pi/c)$ in three configurations: 1) equilibrium ($c=c_o$, where c_o is the optimal length of the supercell in the z -axis direction); 2) elongated ($c=1.005c_o$); and 3) contracted ($c=0.995c_o$). We firstly relax each configuration, and then calculate their phonon dispersions based on $61k$ points in their Brillouin zones. The phonon computation is implemented using the VIBRA package of SIESTA. All structures and vibration modes are visualized in XCRYSDEN software [34].

3 Thermal properties of the BNTs

The band gap and lattice constant of α -boron [16, 17, 35] are calculated to confirm the accuracy of the relevant parameters for BNTs. We obtain an indirect energy band gap of 1.51eV and a lattice parameter of 5.05\AA , which agree with the literature values [38, 39]. Armchair (n,n) BNTs ($n=3-9$) and zigzag ($n,0$) BNTs ($n=3-10$) are considered here. The optimized structures of (3,0) and (3,3) BNTs from the top view are shown in Fig. 1(a). The surface of the optimized BNT is buckled, which is in accordance with the Aufbau principle [40]. The buckling degree decreases as tube diameter increases. In the right part of Fig. 1(a), we also show the corresponding α -boron sheet ($\eta=1/9$) [16], which is assumed as the precursor of a BNT. The diameter dependence of the binding energy is presented in Fig. 1(b). It can be seen that the binding energy increases with diameter, which is consistent with known results [14–16]. The results of the tests of the structural properties further indicate the accuracy of our simulation, and the calculation of the structural configuration is also helpful in understanding their thermal expansion.

For an isotropic crystalline solid, the linear TEC α is calculated by [41]:

$$\alpha = \frac{\sum_{\lambda\kappa} c_{\lambda\kappa} \gamma_{\lambda\kappa}}{3VB}, \quad (3.1)$$

where $c_{\lambda\kappa}$ is the heat capacity of the phonon mode with wave vector κ in the band labeled by λ , V is the tube volume, B is the bulk modulus, and $\gamma_{\lambda\kappa}$ is the mode-dependent

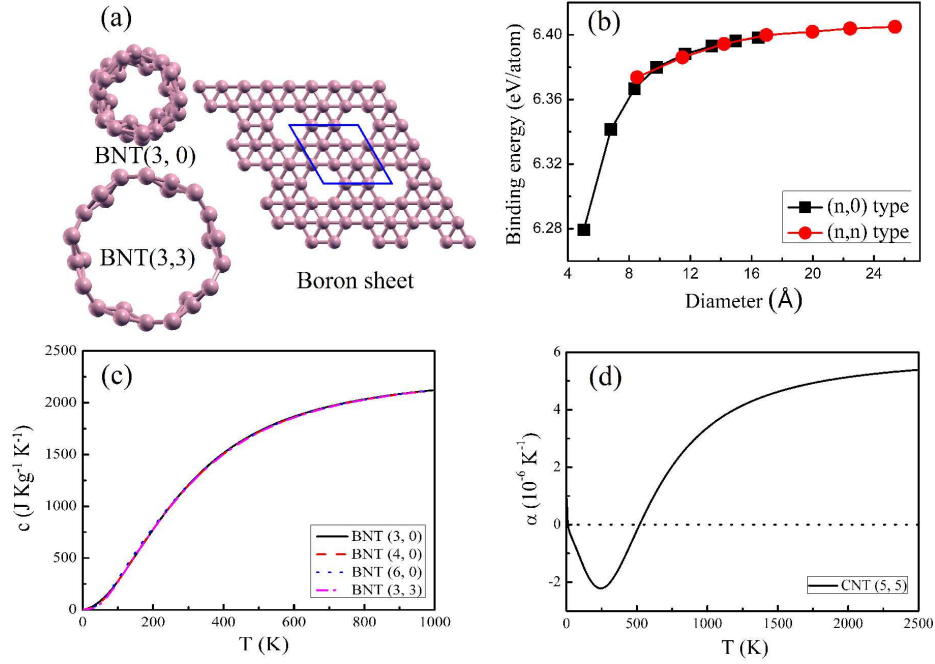


Figure 1: (a) (color online) The left part are the structures of (3,0) and (3,3) BNTs from the top-view. The right part is the top-view of α -boron sheet, and the sheet unit cell is denoted in a quadrilateral. (b) Diameter dependence of the binding energy of the BNTs. The line in black denotes the binding energy of the zigzag BNTs (square one), while the red line denotes the one of the armchair BNTs (circle one). (c) The specific heats of the (3,0), (4,0), (6,0) and (3,3) BNTs. (d) Temperature dependence of linear TEC of the (5,5) CNT.

Grüneisen parameters (GP). The GP are expressed as:

$$\gamma_{\lambda\kappa} = -\frac{V}{\omega_{\lambda\kappa}} \frac{\partial \omega_{\lambda\kappa}}{\partial V}, \quad (3.2)$$

where $\omega_{\lambda\kappa}$ is the phonon frequency. The tube volume is defined as:

$$V = \pi \cdot (a^2 - b^2) \cdot l, \quad (3.3)$$

where a and b are the outer and inner diameters and l is the tube length. The difference between a and b is 3.40Å for a single-walled CNT [42]. The theoretical value of the thickness of the single-walled BNT is 2.98Å or 3.02Å [43]. The interlayer spacing in the multi-walled BNT has been measured as 3.20Å [6]. In our calculation, we adopt this experimental result to denote the wall thickness of single-walled BNT.

The bulk modulus B is defined as:

$$B = V \left(\frac{d^2 U}{dV^2} \right)_{V_0}, \quad (3.4)$$

Table 1: The structural parameters of the investigated nanotubes. The second, third and fourth columns are the tube diameter, volume and bulk modulus respectively. The fifth column is the maximum electron density in the tube.

Tube	Diameter (Å)	Volume (Å ³)	Bulk modulus (GPa)	Maximum electronic density (a.u)
CNT(5,5)	6.904	182.443	168.286	0.3102
BNT(3,0)	4.936	433.315	72.337	0.1386
BNT(4,0)	6.557	579.222	96.372	0.1356
BNT(6,0)	9.803	869.336	125.503	0.1344
BNT(3,3)	8.478	434.418	91.907	0.1348

where U is the internal energy, and V_0 is the tube volume at the ground state. The Birch-Murnaghan equation of state to the second order is selected to calculate the bulk modulus of each tube. The relevant parameters given above are calculated and given in Table 1; the bulk modulus of (5,5) CNT is 168.3GPa, which agrees with the result of Lu et al. [17]. Given the same tube chirality, the bulk modulus of BNT increases with the increasing diameter.

According to Eq. (3.1), we calculate the specific heat for each tube using the following expression:

$$c = \frac{1}{mN_{\kappa}} \sum_{\kappa,\lambda} \left[k_B \left(\frac{\hbar\omega_{\kappa\lambda}}{k_B T} \right)^2 \frac{e^{\hbar\omega_{\kappa\lambda}/k_B T}}{(e^{\hbar\omega_{\kappa\lambda}/k_B T} - 1)^2} \right], \quad (3.5)$$

where m is the mass of unit cell of each nanotube and N_{κ} is the number of K -points. The specific heats of different BNTs are shown in Fig. 1(c). It can be seen that the specific heat is independent of size and chirality and increases with increasing temperature. A value of $1.206 \times 10^3 \text{J} \cdot \text{kg}^{-1} \cdot \text{K}^{-1}$ is found at room temperature. A large specific heat would be helpful in fabricating high-quality BNT based nanodevices for nanoscale thermal management.

After all the useful parameters in Eq. (3.1) have been obtained, we can begin to study the TEC of each BNT using an approach based on the phonon frequency [27]. Eq. (3.1) could be rewritten as:

$$\alpha = \frac{1}{3B} \left\{ \frac{1}{N_k} \sum_{k,\lambda} \left[\left(-\frac{\hbar\Delta\omega_{k\lambda}}{\Delta V} \right) \frac{\hbar\omega_{k\lambda}}{k_B T^2} \frac{e^{\hbar\omega_{k\lambda}/k_B T}}{(e^{\hbar\omega_{k\lambda}/k_B T} - 1)^2} \right] \right\}, \quad (3.6)$$

where $\Delta\omega_{\kappa\lambda}$ and ΔV are the differences of phonon frequency and volume between the equilibrium and strained tubes. For the thermal expansion of the CNTs, Maniwa et al. reported a radial TEC of $(-0.15 \pm 0.20) \times 10^{-5} \text{K}^{-1}$ for CNT bundles by x -ray diffraction [44]. The TEC of a single-walled (5,5) CNT has been calculated to be $3.84 \times 10^{-6} \text{K}^{-1}$ using a molecular dynamics simulation and a lattice dynamic calculation based on the empirical bond-order potential [28]. Our result for the linear TEC of (5,5) CNT according to Eq. (3.6) is shown in Fig. 1(d). The negative TEC with the maximum absolute value, $-2.211 \times 10^{-6} \text{K}^{-1}$ appears at 243K, while the largest TEC is $5.384 \times 10^{-6} \text{K}^{-1}$ occurring at

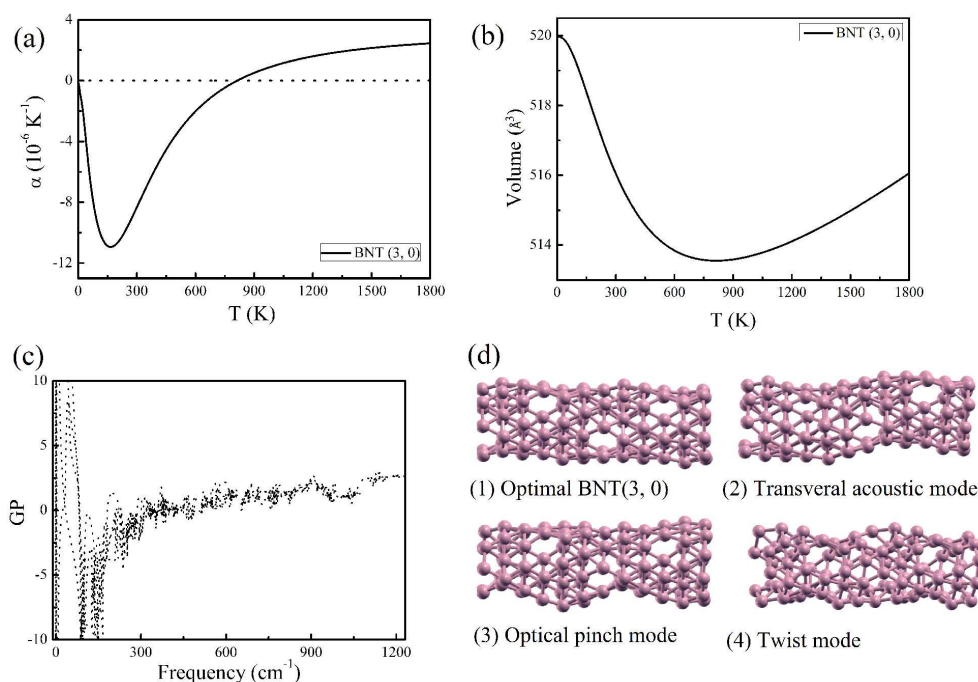


Figure 2: (a) Temperature dependence of the linear TEC of the (3,0) BNT. (b) The volume change of the (3,0) BNT with increasing temperatures. (c) The GP versus phonon frequency of the (3,0) BNT. (d) Some of low frequency vibration modes: (1) the optimal (3,0) BNT with two units from the side-view; (2) the transversal acoustic mode; (3) the optical pinch mode; (d) the twist mode.

2500K. The values obtained are close to the results reported, confirming the method as reliable.

Having checked the method, the TECs of BNTs can now be investigated. For clarity, we first discuss the TEC of (3,0) BNT in detail. Fig. 2(a) shows the relationship between the TEC of the (3,0) BNT and the temperature. The TEC decreases first, and the negative TEC with the maximum absolute value, $-1.094 \times 10^{-5} \text{K}^{-1}$ is achieved at 166K, which absolute value is much larger than that of $-2.211 \times 10^{-6} \text{K}^{-1}$ in the (5,5) CNT. Since the linear TEC is defined as $\alpha = (3V)^{-1} \partial V / \partial T$, we can obtain that $V(T) = V_0 \exp(\int_0^T 3\alpha dT)$. Fig. 2(b) presents the volume change of (3,0) tube with increasing temperatures. The large negative TEC indicates an opportunity for the application of BNTs in actuators and memory materials. Additionally, they would be useful in counterweighing the thermal expansion of other materials in a BNT-based nanodevice. As the temperature increases, the TEC of (3,0) BNT moves from negative to positive, and a value of $2.449 \times 10^{-6} \text{K}^{-1}$ is achieved at 1800K.

Previous theoretical studies have proposed that the thermal contraction of CNT is caused by the transversal vibration modes [32]; while the thermal expansion is due to high longitudinal vibration modes leading to bond expansion [29]. To investigate the ori-

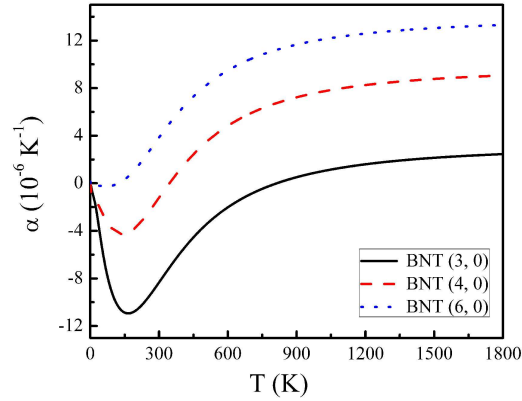


Figure 3: Temperature dependence of the LTECs of BNTs with different tube diameters, the TECs of (3,0), (4,0) and (6,0) BNTs are denoted in solid black, dash red and dot blue line respectively.

gin of the thermal expansion of (3,0) BNT, we follow the literatures and focus on its various vibration modes. According to Eq. (3.1), the TEC varies directly with the GP and heat capacity. As we know the specific capacity is positive and independent of tube diameter and chirality, a negative or positive GP indicates the effect of the corresponding vibration mode on thermal contraction or expansion. Accordingly, we investigate its vibration modes combined with its GP. The GP of the (3,0) BNT is provided in Fig. 2(c). Here, we find that the negative GPs appear mainly in the low phonon frequency region, particularly below 200cm^{-1} . The corresponding excitation temperature $T = \hbar\omega/k_B$ should be 288K. As shown in Fig. 2(a), there is a large negative TEC at this temperature, indicating that the corresponding vibration modes with phonon frequency below 200cm^{-1} induce prominent thermal contraction. These modes are visualized using XCRYSDEN code. They are mainly the transversal vibration modes, such as transversal acoustic bending, optical pinch, and twist modes. We show these three types in Fig. 2(d). As the phonon frequency increases in Fig. 2(c), positive GPs are found in the high-frequency area. Correspondingly, the TEC shifts from negative to positive with increasing temperature. Similar to the situation reported in [29], this is mainly due to the excitation of the high-frequency longitudinal vibration modes as the temperature increases. The anharmonicity of the interatomic potential increases the bond length. The bond expansion overwhelms the thermal contraction caused by the low-frequency vibration modes.

To explore the effect of size on thermal expansion, we also study the temperature dependence of the TECs of (3,0), (4,0) and (6,0) BNTs. These are presented in Fig. 3. The TEC is significantly sensitive to the tube diameter. The (3,0) BNT has the largest thermal contraction, as discussed above. The (4,0) BNT contracts with negative TEC till 345K and the negative TEC with the largest absolute value is $-4.273 \times 10^{-6} \text{K}^{-1}$. It expands with a TEC of approximately $9.065 \times 10^{-6} \text{K}^{-1}$ at high temperatures. The TEC of (6,0) BNT is negative when the temperature is below 123K. The largest TEC is nearly $1.331 \times 10^{-5} \text{K}^{-1}$.

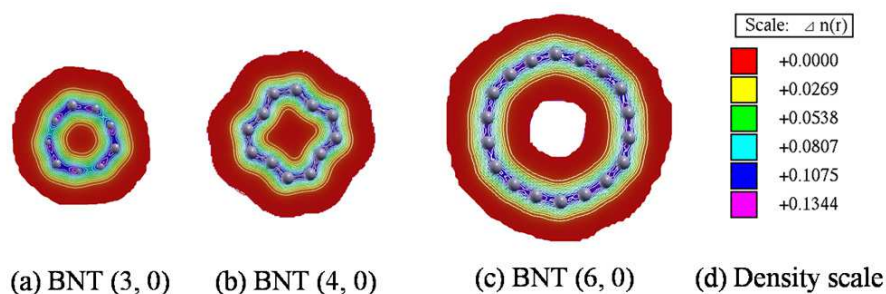


Figure 4: The electron density distribution maps from the top view: (a) BNT (3,0); (b) BNT (4,0); (c) BNT (6,0); (d) the electron density scale.

Comparing the three tubes reveals that the TEC increases with diameter. We also find the thermal contraction disappears at larger tube sizes. As discussed in [30], thinner tubes exhibit more flexibility and contract more in the axial direction. This is also confirmed by our results. In other words, the amplitude of the low-frequency transversal vibration mode is more significant when the tube diameter is small. Based on our study of these structural properties, we can conclude that the surface buckling degree is lower at larger diameters, and the binding energy increases with the diameter. Logically, the diameter dependence of the TECs is correlated with the structural differences. To investigate the proximate cause, the charge density maps of these tubes are visualized using XCRYSDEN software. The maximum density of the electron states are presented in Table 1. For the BNTs, the maximum density value of the electron states decreases with increasing tube diameter, whereas the electron number increases. Therefore, the electron density is more localized at smaller diameters as well as when the surface is more buckled. With the sp^2 hybridization of its orbital, the BNT possesses a delocalized π bond. As a result, the electron will construct a stronger delocalized π bond at larger diameters with a smoother surface. This can be seen from Fig. 4. As is already well known, a strong delocalized π bond enlarges the material's mechanical strength, which is consistent with the increased bulk modulus of BNTs reported here. Within the quasi-harmonic approximation, the vibration energy satisfies $E = AX^2/2$ (where A is a fitting parameter proportional to its mechanical properties and X is the vibration amplitude). At a constant temperature T , the transversal vibration amplitude ($X = \sqrt{2k_B T/A}$) is larger with smaller A . Consequently, the thermal contraction will be more obvious at smaller tube diameters.

So far we have studied the size effect on the TECs of BNTs. In the next part, we extend our discussion to the chirality effect. The TECs of (3,0) and (3,3) BNTs are investigated and presented in Fig. 5. As can be seen, the thermal contraction of the (3,0) tube is more obvious than the one of the (3,3) BNT in the low-temperature region. However, the thermal expansion of the (3,0) surpasses that of the (3,3) tube at higher temperatures. To understand this interesting pattern of thermal expansion, we need to examine their structural differences. The tube diameter of (3,0) is smaller than that of the (3,3) tube. Due to their different chiralities, although the atom number per unit cell of the (3,0)

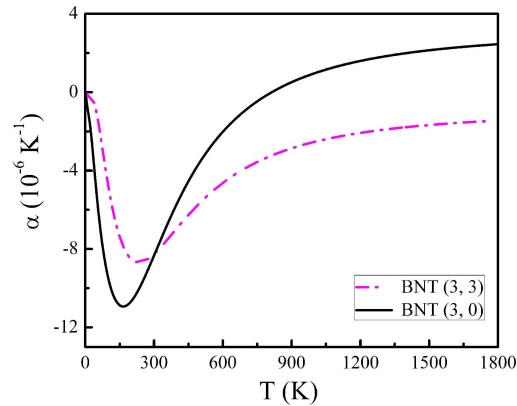


Figure 5: Temperature dependence of the LTECs of BNTs with different tube chiralities, the LTECs of the (3,0) and (3,3) BNTs are denoted in solid black and dash dot magenta line respectively.

and (3,3) BNTs is equivalent, the bulk modulus and surface buckling are different. At low temperatures, only the low-frequency transversal vibration modes are excited. The amplitude of the transversal vibration modes of the (3,0) BNT is larger due to its smaller diameter. Consequently, the thermal contraction is more prominent in the (3,0) tube. As the temperature increases, the longitudinal vibrations causing bond expansion are excited. Due to the more buckled surface and smaller bulk modulus, the bond expansion is more evident in (3,0) tube. The TEC of the (3,0) tube surpasses that of the (3,3) around room temperature. The low-frequency vibration mode causes thermal contraction and the bond expansion causes thermal expansion, which explains our results well.

4 Conclusions

In conclusions, among the various thermal properties of the single-walled BNT, the specific heat is not dependent on either tube diameter or chirality. In contrast, the TEC depends on those two factors, as a result of the interaction between the thermal contraction caused by low-frequency transversal vibration modes and the thermal expansion due to longitudinal vibration modes. Given the same tube chirality and the smaller tube diameter (and thus the weaker delocalized π bond) the thermal contraction is more prominent. At different chiralities, the thermal contraction in low temperature and the thermal expansion in high temperature in (3,0) tube are more evident than those of (3,3) tube. The notable thermal contraction of (3,0) BNT would make it useful in applications such as sensors, memory materials, or actuators, or even in counterweighing the thermal expansion of other materials combined in BNT-based devices. These predominant structural, electronic, and thermal properties indicate that BNTs have potential applications in nanotechnology. Our work therefore facilitates the development of high-performance BNT-based devices.

Acknowledgments

The work described in this paper was supported by grants from the National Basic Research Program of China (973 Program Grant No. 2012CB215405), the National Natural Science Foundation of China (Grant No. 11374272), and City University of Hong Kong (Project No. 7008092). This research was conducted partially using the resources of the High Performance Cluster Computing Centre, Hong Kong Baptist University, which receives funding from Research Grant Council, University Grant Committee of the HKSAR and Hong Kong Baptist University.

References

- [1] S. Iijima, Helical microtubules of graphitic carbon, *Nature (London)*, 354 (1991), 56–58.
- [2] G. Overney, W. Zhong and D. Tománek, Structural rigidity and low frequency vibrational modes of long carbon tubules, *Z. Phys. D*, 27 (1993), 93–96.
- [3] S. Iijima, C. Brabec, A. Maiti and J. Bernholc, Structural flexibility of carbon nanotubes, *J. Chem. Phys.*, 104 (1996), 2089–2092.
- [4] J. Lu, Elastic properties of single and multilayered nanotubes, *J. Phys. Chem. Solids*, 58 (1997), 1649–1652.
- [5] Y. Xu, H. Peng, R. H. Hauge and R. E. Smalley, Controlled multistep purification of single-walled carbon nanotubes, *Nano Lett.*, 5 (2005), 163–168.
- [6] F. Liu, C. Shen, Z. Su, X. Ding, S. Deng, J. Chen, N. Xu and H. Gao, Metal-like single crystalline boron nanotubes: synthesis and in situ study on electric transport and field emission properties, *J. Mater. Chem.*, 20 (2010), 2197–2205.
- [7] V. I. Matkovich, *Boron and Refractory Borides*, Springer, New York, 1977.
- [8] D. Ciuparu, R. F. Klie, Y. Zhu and L. Pfefferle, Synthesis of pure boron single-wall nanotubes, *J. Phys. Chem. B*, 108 (2004), 3967–3969.
- [9] M. H. Evans, J. D. Joannopoulos and S. T. Pantelides, Electronic and mechanical properties of planar and tubular boron structures, *Phys. Rev. B*, 72 (2005), 045434(6).
- [10] J. Kunstmann and A. Quandt, Constricted boron nanotubes, *Chem. Phys. Lett.*, 402 (2005), 21–26.
- [11] J. Kunstmann and A. Quandt, Broad boron sheets and boron nanotubes: an *ab initio* study of structural, electronic, and mechanical properties, *Phys. Rev. B*, 74 (2006), 035413(14).
- [12] K. C. Lau and R. Pandey, Stability and electronic properties of atomistically-engineered 2D boron sheets, *J. Phys. Chem. C*, 111 (2007), 2906–2912.
- [13] I. Cabria, M. J. López and J. A. Alonso, Density functional calculations of hydrogen adsorption on boron nanotubes and boron sheets, *Nanotechnology*, 17 (2006), 778–785.
- [14] H. Tang and S. Ismail-Beigi, Novel precursors for boron nanotubes: the competition of two-center and three-center bonding in boron sheets, *Phys. Rev. Lett.*, 99 (2007), 115501(4).
- [15] X. Yang, Y. Ding and J. Ni, *Ab initio* prediction of stable boron sheets and boron nanotubes: structure, stability, and electronic properties, *Phys. Rev. B*, 77 (2008), 041402(4).
- [16] H. Tang and S. Ismail-Beigi, First-principles study of boron sheets and nanotubes, *Phys. Rev. B*, 82 (2010), 115412(20).
- [17] H. Lu, Y. Mu, H. Bai, Q. Chen and S. D. Li, Binary nature of monolayer boron sheets from *ab initio* global searches, *J. Chem. Phys.*, 138 (2013), 024701(4).

- [18] V. Bezugly, J. Kunstmann, B. Grundkötter-Stock, T. Frauenheim, T. Niehaus and G. Cuniberti, Highly conductive boron nanotubes: transport properties, work functions, and structural stabilities, *ACS Nano*, 5 (2011), 4997–5005.
- [19] X. Wu, J. Dai, Y. Zhao, Z. Zhuo, J. Yang and X. C. Zeng, Two-dimensional boron monolayer sheets, *ACS Nano*, 6 (2012), 7443–7453.
- [20] A. K. Singh, A. Sadrzadeh and B. I. Yakobson, Probing properties of boron α -tubes by *ab initio* calculations, *Nano Lett.*, 8 (2008), 1314–1317.
- [21] K. C. Lau, R. Pandey and R. Pati, Theoretical study of electron transport in boron nanotubes, *Appl. Phys. Lett.*, 88 (2006), 212111(3).
- [22] J. Zhu, C. M. Andres, J. Xu, A. Ramamoorthy, T. Tsotsis and N. A. Kotov, Pseudonegative thermal expansion and the state of water in graphene oxide layered assemblies, *ACS Nano*, 6 (2012), 8357–8365.
- [23] W. Kohn and L. J. Sham, Self-consistent equations including exchange and correlation effects, *Phys. Rev.*, 140 (1965), 1133–1138.
- [24] P. Ordejon, E. Artacho and J. M. Soler, Self-consistent order- N density-functional calculations for very large systems, *Phys. Rev. B*, 53 (1996), 10441–10444.
- [25] J. M. Soler, E. Artacho, J. D. Gale, A. García, J. Junquera, P. Ordejón and D. Sánchez-Portal, The SIESTA method for *ab initio* order- N materials simulation, *J. Phys. Condens. Matter*, 14 (2002), 2745–2779.
- [26] J. P. Perdew, K. Burke and M. Ernzerhof, Generalized gradient approximation made simple, *Phys. Rev. Lett.*, 77 (1996), 3865–3868.
- [27] S. Baroni, S. de Gironcoli and A. D. Corso, Phonons and related crystal properties from density-functional perturbation theory, *Rev. Mod. Phys.*, 73 (2001), 515–562.
- [28] M. U. Kahaly and U. V. Waghmare, Size dependence of thermal properties of armchair nanotubes: a first-principles study, *Appl. Phys. Lett.*, 91 (2007), 023112(3).
- [29] P. K. Schelling and P. Keblinski, Thermal expansion of carbon structures, *Phys. Rev. B*, 68 (2003), 035425(7).
- [30] G. Cao, X. Chen and J. W. Kysar, Apparent thermal contraction of single-walled carbon nanotubes, *Phys. Rev. B*, 72 (2005), 235404(6).
- [31] H. Jiang, B. Liu, Y. Huang and K. C. Hwang, Thermal expansion of single wall carbon nanotubes, *J. Eng. Mater. Technol.*, 126 (2004), 265–270.
- [32] Y. Kwon, S. Berber and D. Tománek, Thermal contraction of carbon fullerenes and nanotubes, *Phys. Rev. Lett.*, 92 (2004), 015901(4).
- [33] P. Giannozzi, S. de Gironcoli, P. Pavone and S. Baroni, *Ab initio* calculation of phonon dispersions in semiconductors, *Phys. Rev. B*, 43 (1991), 7231–7242.
- [34] A. Kokalj, XCrySDen—a new program for displaying crystalline structures and electron densities, *J. Mol. Graph. Model.*, 17 (1999), 176–179.
- [35] M. Fujimori, T. Nakata, T. Nakayama, E. Nishibori, K. Kimura, M. Takata and M. Sakata, Peculiar covalent bonds in α -rhombohedral boron, *Phys. Rev. Lett.*, 82 (1999), 4452–4455.
- [36] N. Vast, S. Baroni, G. Zerah, J. M. Besson, A. Polian, M. Grimsditch and J. C. Chervin, Lattice dynamics of icosahedral α -boron under pressure, *Phys. Rev. Lett.*, 78 (1997), 693–696.
- [37] S. Shang, Y. Wang, R. Arroyave and Z. Liu, Phase stability in α - and β -rhombohedral boron, *Phys. Rev. B*, 75 (2007), 092101(4).
- [38] A. Masago, K. Shirai and H. Katayama-Yoshida, Crystal stability of α - and β -boron, *Phys. Rev. B*, 73 (2006), 104102(10).
- [39] D. Li, Y. Xu and W. Y. Ching, Electronic structures, total energies, and optical properties of α -rhombohedral B_{12} and α -tetragonal B_{50} crystals, *Phys. Rev. B*, 45 (1992), 5895–5905.

- [40] I. Boustani, Systematic *ab initio* investigation of bare boron clusters: determination of the geometry and electronic structures of B_n ($n=2-14$), *Phys. Rev. B*, 55 (1997), 16426–16438.
- [41] E. T. Thostenson, Z. Ren and T. Chou, Advances in the science and technology of carbon nanotubes and their composites: a review, *Compos. Sci. Technol.*, 61 (2001), 1899–1912.
- [42] A. Krishnan, E. Dujardin, T. W. Ebbesen, P. N. Yianilos and M. M. J. Treacy, Young's modulus of single-walled nanotubes, *Phys. Rev. B*, 58 (1998), 14013–14019.
- [43] I. Boustani, A. Quandt, E. Hernandez and A. Rubio, New boron based nanostructured materials, *J. Chem. Phys.*, 110 (1999), 3176–3185.
- [44] Y. Maniwa, R. Fujiwara, H. Kira, H. Tou, H. Kataura, S. Suzuki and Y. Achiba, Thermal expansion of single-walled carbon nanotube (SWNT) bundles: X-ray diffraction studies, *Phys. Rev. B*, 64 (2001), 241402(3).